A Cerenkov Microlaser

E. Fisch, Albert K. Henning, *Member, IEEE,* and J. Walsh

***Abstract*—A Cerenkov microlaser (CML) is proposed. The device will use an electron beam and a semiconducting-film-loaded open, quasi-optical resonator to produce coherent, electromagnetic radiation at submm and far-infrared wavelengths. General expressions for the tuning, gain, and constraints due to beam quality are used, together with optical and material considerations to establish operating characteristics.**

I. Introduction

A Cerenkov microlaser (CML) design is proposed. These devices use an electron beam moving over the surface of a semiconducting film to produce coherent electromagnetic radiation. The anticipated operating range is the submm-FIR region of the spectrum and the electron beam energies required are modest (20–200 kV). The CML is similar to devices which have been operated successfully with low-index-of-refraction materials, such as quartz [1], boron nitride [2], polyethylene [3], and TPX [4]. The Cerenkov threshold energy increases as the relative dielectric constant of the film material decreases, and thus high-energy beams (hundreds of kV–MV) have been used in these experiments. In both the low and high electron beam energy limits, the basic theory of operation is the same. An electron moving near the film surface at a velocity exceeding that of light in the film material, emits both spontaneous and stimulated Cerenkov radiation. A portion of the stimulated Cerenkov radiation is trapped in a resonator formed by mirrors which terminate a length of surface waveguide. If the gain is sufficient, a coherent Cerenkov wave grows to saturation. The use of higher-index semiconducting materials for the surface guide reduces the beam energy required and leads to a physically smaller device, which is attractive for many applications. A further advantage of the semiconducting films lies in the fact that their dc conductivity is large enough to eliminate problems associated with charge buildup on the film surface.

This paper is divided into four sections. The basic theory of operation will be summarized in Section II and resonator optics will be discussed in Section III. These results will then be used to evaluate the design characteristics of the CML. General conclusions are presented in Section IV.

II. Cerenkov Laser Theory

The basic Cerenkov laser mechanism is illustrated in Fig. 1. An electron moving above and parallel to the surface of a film of dielectric constant ϵ, with a velocity $(c\beta_o)$ which is greater than the speed of light in the film material (c/ϵ), will produce a spontaneous Cerenkov radiation wake. When mirrors are added, forming a resonator, the stimulated Cerenkov radiation will increase the stored energy in the fields. If the resonator Q is sufficient, a coherent oscillation will grow until nonlinear effects cause saturation. The general theory of these devices has been discussed in a number of places [5], [6] and hence, only a brief summary will be presented here. The central issues are dispersion and tuning, coupling and gain, the constraints imposed by beam quality, and nonlinear saturation. These will be addressed in order. Throughout the paper three common semiconductor film materials were chosen to illustrate the theory: Si, GaAs, and Ge. They have real dielectric constants of 11.8, 12.9, and 16.0 in the FIR. The imaginary part of the dielectric constants are largely sample-dependent and small; they are not included in the FEL theory, but are indicative of resonator losses associated with the film.

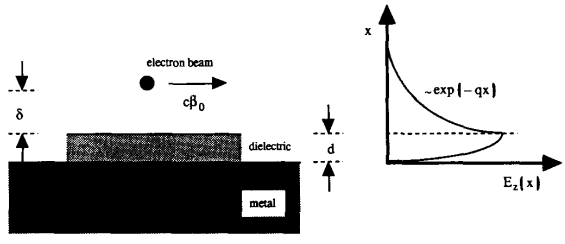

Fig. 1. The Cerenkov laser mechanism is shown schematically. An electron passes a distance δ from a thin dielectric slab. The z component of the electric field to which it couples is also shown.

Dispersion and Tuning

The electron beam couples predominantly to the longitudinal electric field, or to the TM cavity modes. In the case of the structure illustrated in Fig. 1, the dispersion function for these modes takes the form [6]

$$D\left(\frac{\omega d}{c}, kd\right) = pd \tan pd - \epsilon qd \tag{1}$$

where $\omega d/c$ and kd are the angular frequency and axial wavenumber scaled in units of film thickness d. The other variables,

$$p^2 = \frac{\omega^2\epsilon}{c^2} - k^2 \tag{2a}$$

and

$$q^2 = k^2 - \frac{\omega^2}{c^2} \tag{2b}$$

are the transverse wavenumbers in the film (of dielectric constant ϵ) and vacuum regions, respectively. The solutions on the $\omega d/c - kd$ plane determined from $D = 0$ are illustrated in Fig. 2. Three film materials, Ge, GaAs, and Si, and two branches of $D = 0$, are shown. At long wavelengths ($\omega d/c \to 0$) the dispersion relation of the lowest-order mode becomes asymptotic to the speed of light in vacuum. As $\omega d/c$ increases, the

Manuscript received May 3, 1990; revised January 14, 1991.

The authors are with the Department of Physics and Astronomy, Dartmouth College, Hanover, NH 03755.

IEEE Log Number 9143431.

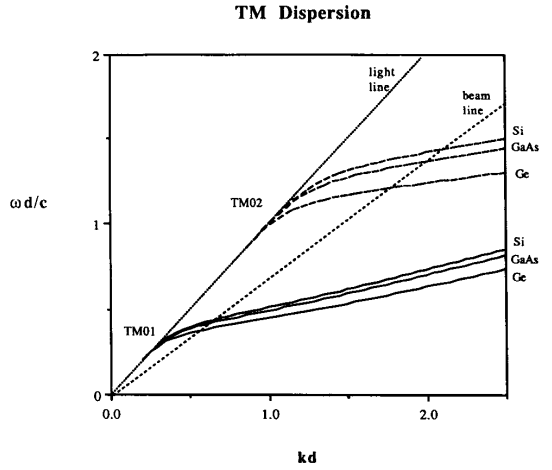

Fig. 2. The TM_{01} and TM_{02} solutions to $D(\omega d/c, kd, \epsilon) = 0$ are shown for the three dielectric constants corresponding to Si, GaAs, and Ge. The light line and beam lines indicate the phase velocity of the light in vacuum and the beam velocity, respectively. Synchronism occurs at intersections of the beam line and the dispersion relation.

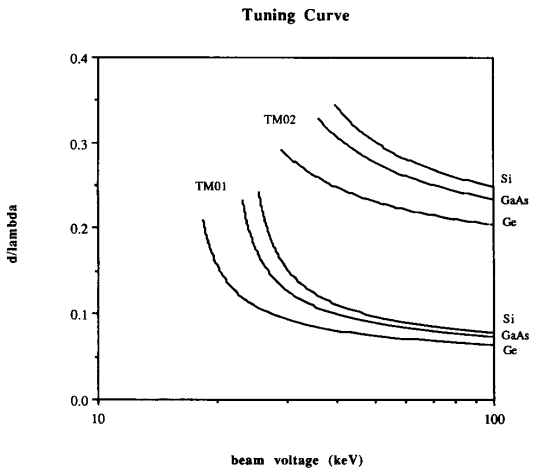

Fig. 3. The tuning curve is shown for the lowest order TM modes of Si, GaAs, and Ge. This plot of dielectric thickness–output wavelength versus beam voltage is generated from the dispersion relation by imposing the synchronism condition.

phase velocity of the wave decreases. Eventually the dispersion relation becomes asymptotic to the speed of light in the dielectric. The evanescence scale length (q^{-1}) decreases continuously along this trajectory. Higher-order branches of $D = 0$ begin on the vacuum light line at points where $\omega d/c = n\pi$ and exhibit the same trends as the fundamental branch.

The spontaneous emission peaks at e-beam-wave synchronism, which is defined by

$$\frac{\omega}{k} = c\beta_o. \tag{3}$$

The stimulated emission rate (growth) will peak at a point near but slightly below this point. Solving $D = 0$ at synchronism determines the tuning function

$$D_T\left(\frac{\omega d}{c}, \frac{\omega d}{c\beta}, \epsilon\right) = 0. \tag{4}$$

The tuning curves corresponding to the dispersion relations of Fig. 2 are shown in Fig. 3. The additional dispersion of the material is not included since it would unnecessarily complicate the theory: the general dependence on ϵ is clear from the family of curves. When the value of ϵ is fixed, D_T is a universal function of the scaled frequency and wavenumber. Thus, one of two general scaling relations for the CML is given by

$$\lambda \sim d. \tag{5}$$

Since d may become small, short-wavelength operation presents no difficulty in principle.

Gain

FEL gain is generally considered to be single-particle or collective, depending on the density of the electron beam. To minimize the requirements of the electron beam source, we consider the former, with beam current densities 10's of A/cm^2 or less. In this case there will be less than one beam plasma oscillation in a resonator length. The effect of the beam on the optical field in the resonator may be defined in terms of an active Q:

$$\frac{1}{Q_b} \equiv \frac{\int \underline{J}^* \cdot \underline{E}\, dV}{1/2\omega\mathcal{E}} \tag{6}$$

where $\underline{J}$ is the modulated current produced by the electric field $\underline{E}$ and $\mathcal{E}$ is the energy stored in the resonator. The numerator on the right-hand side of (6) is the work done on the particle by the field.

At small to moderate current densities, the gain during the time (τ) it takes a single electron to traverse the resonator (length L, $\tau = L/c\beta_o$) is given by

$$g = -\frac{\omega\tau}{Q_b} \tag{7}$$

where the negative sign in (7) occurs because the field energy increases (positive gain) in regions where $1/Q_b < 0$. The evaluation of (6) can be approached in a variety of ways. The anticipated e-beam energy is modest and hence, a strong axial magnetic field will be used to render the electron motion effectively one-dimensional. It is a simple matter to use particle equations of motion, in the vacuum fields of the guide, to evaluate the energy lost per electron. The numerator on the RHS of (6) can be reexpressed as

$$\frac{1}{2}\int \underline{J}^* \cdot \underline{E}\, dV = \frac{mc^2}{e}\int_{\text{beam}} dA\, J_b(r_b)\, \overline{\delta\gamma}(L, x_o) \tag{8}$$

where $J_b(r_b)$ is the cross section of the beam and $\overline{\delta\gamma}(L, x_o)$ is the phase-averaged electron energy loss. The energy input rate follows directly. Since the beam is treated as a perturbation, the vacuum fields can be used to evaluate the stored energy. The gain per pass for a beam of width σ_{by}, traversing a resonator with mode width w, becomes

$$g = \frac{J_{bo}L^2}{(mc^3/e)} \cdot \frac{\sigma_{by}}{w} \cdot \frac{L}{d} \cdot f_c g_o \tag{9}$$

where J_{bo} is the peak beam current density, (mc^3/e = 17 kA) f_c is a coupling factor, d is the film thickness, and

$$g_o = \frac{8\pi(\gamma^2 - \gamma_T^2)}{\beta^5\gamma^7} \frac{kdF_R(\kappa L)}{\left[1 + \frac{kd}{\gamma}\left(1 + \frac{\epsilon}{\gamma^2}\right)\right]} \tag{10}$$

contains all of the factors in the gain which scale in a universal manner along $D = 0$. Synchronism, ($\beta = \omega d/ckd$, $\gamma = 1/\sqrt{1 - \beta^2}$) is assumed, and $\gamma_T = \sqrt{\epsilon/(\epsilon - 1)}$ is the relative energy at the Cerenkov threshold. In evaluating (10), the functional dependence of $\beta(kd)$ and $\gamma(kd)$ along the dispersion must be observed. Thus, as $kd \to 0$, $\gamma(kd) \to \infty$ and gain will vanish as $kd \to 0$. This limit applies if either k or $d \to 0$. It also should be noted in passing that evaluation of the gain in the collective limit, since the analysis outlined in [6], would lead to a generally similar grouping of the beam and resonator parameters.

The single particle gain line shape, $F_R(\kappa L)$ (Fig. 4), is given by

$$F_R(\kappa L) = \frac{2(1 - \cos \kappa L) - \kappa L \sin \kappa L}{(\kappa L)^3} \tag{11}$$

where

$$\kappa L \equiv \left(k - \frac{\omega}{c\beta_o}\right)L \tag{12}$$

is the relative slippage between the wave and a beam electron. The gain peaks at $\kappa L = 2.34$ and $F_R = -0.135$ at that point. Plots of the value of $-g_o$ at the point of maximum gain are displayed on the same axes as the tuning curve (Fig. 5).

Beam Quality

The width of the gain line determines the minimum acceptable electron energy spread. A schematic representation of a beam distribution is shown in Fig. 4. All electron beam dephasing effects are assumed to originate from a longitudinal velocity spread. A comparison of the two curves in Fig. 4 shows that the electron phase spread must be such that

$$\overline{k\delta v L/c\beta_o} < \kappa L. \tag{13}$$

The κL axis in Fig. 4 indicates that a phase spread of π or less is reasonable. Incorporating this limit, assuming that energy fluctuations cause the velocity spread, (13) becomes

$$\frac{\delta V_{\text{beam}}}{V_{\text{beam}}} < \frac{\lambda\gamma}{2L}(\gamma + 1). \tag{14}$$

Coupling

The function f_c, which appears in the expression for g, is a dimensionless measure of coupling: a filling factor. It depends upon the beam cross section and the mode profile. As a first approximation it is convenient to assume that the distribution is rectangular with thickness σ_{bx} and a lower edge located a distance δ above the surface. For this case [6],

$$f_c = e^{-\mu_\delta}(1 - e^{-\mu_c}) \tag{15}$$

where the dimensionless coupling parameters

$$\mu_{c,\delta} = \frac{4\pi(\sigma_{bx} \text{ or } \delta)}{\lambda\beta\gamma} \tag{16}$$

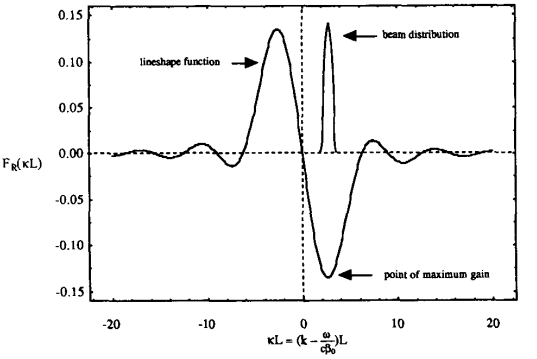

Fig. 4. The single particle line shape function is plotted versus phase mismatch, κL. An approximately monoenergetic beam distribution is also shown to illustrate the permissible degree of phase spread.

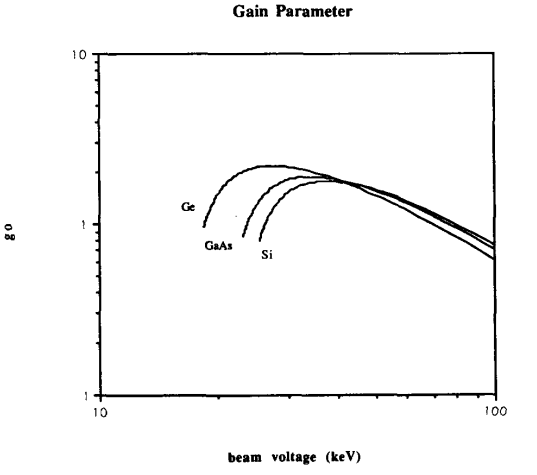

Fig. 5. The gain parameter $-g_0$, is plotted versus beam energy for the TM_{01} mode of Si, GaAs, and Ge. The second branch solutions are larger by a barely discernible amount on this scale.

TABLE I
CML DESIGN SPECIFICATIONS NEEDED TO MAINTAIN g^{-1} FOR SEVERAL WAVELENGTHS. WE SET V_b = 100 kV AND $L/\lambda = 10^2$. THE BEAM-FILM GAP δ AND THE BEAM THICKNESS ARE CALCULATED FOR $\mu_g = 1$ AND $\mu_c = 4$.

λ (μm)	L (cm)	δ (μm)	σ_{bx} (μm)	J_b (A/cm^2)
100	1	2.2	9	460
200	2	4.4	18	115
500	5	11	44	18.4
1000	10	22	88	46

come from the values of $2q\sigma_{bx}$ and $2q\delta$ evaluated at synchronism. The coupling parameters quantify the amount of field energy in the vacuum space above the film: μ increases with shorter x and lower energies, and the net effect on (15) must be evaluated on a case-by-case basis.

A gap size δ, which yields $\mu_\delta = 1$, reduces the gain by a factor $e^{-1} = 0.368$. Values of δ, which must be maintained in order to meet the condition $\mu_\delta = 1$, are listed in Table I. The

factor μ_c is a dimensionless measure of the wave evanescence over the beam profile. In some high-frequency tubes, such as THz carcinotrons, operation with surprisingly large values of μ_c (10–15) are reported. In the present design survey, the more conservative limit $\mu_c \leq 4$ will be assumed and these values are also listed on Table I. The constraints implied by (16) constitute the second general scaling relation for CML design.

III. The CML Resonator

Before treating specific materials and cavity designs, it is useful to establish their effect on CML operation. Consider a dielectric waveguide of length L with material losses α_m and end mirrors characterized by reflectivities r_1 and r_2. The system must have sufficient gain to overcome losses associated with propagation in the guide, or

$$\alpha_{\text{thresh}} = \frac{1}{2}\left(\alpha_m - \frac{1}{L}\ln(r_1 r_2)\right). \tag{17}$$

This can be written in terms of a cavity Q [7] as

$$\frac{1}{Q_{\text{cav}}} = \frac{1}{Q_{\text{diel}}} + \frac{1}{Q_{\text{mirror}}} = \frac{\alpha_m v_g}{\omega} - \frac{v_g}{2L\omega}\ln(r_1 r_2) \tag{18}$$

where v_g is the group velocity, $d\omega/dk$. The group velocity and operating frequency ω are dictated by the excited mode, and are taken from the dispersion relation. The active beam quality of (6) must exceed that of the cavity for lasing. Minimizing $1/Q_{\text{cav}}$ delineates the resonator-dependent areas of concern. The geometric design implications are that L should be large relative to λ. It is also clear that $r_1 r_2$ should be as high as possible while still permitting output coupling. Finally, the material losses should be small. Thus, the four main resonator design issues are: macroscopic dimensions, mode confinement, mirror reflectivity, and material losses.

Macroscopic Dimensions

The infinite planar resonator dispersion relation was shown in Fig. 2. Including finite resonator dimensions (Fig. 6) in the y and z directions imposes additional restrictions on the dispersion [8]. For a guide of width w, length L, and index n_1, the axial wavenumbers of (2) become

$$q^2 = \left(\frac{\omega n_1}{c}\right)^2 - k_{nm}^2$$

$$p^2 = k_{nm}^2 - \left(\frac{\omega}{c}\right)^2 \tag{19}$$

where $k_{nm} = n\pi/L + m\pi/w$. These solutions are longitudinal section magnetic or LSM_{lmn} modes. They reduce to the more specific TM_{1n} solutions when the problem is less constrained. The resultant dispersion is a subset of the one discussed earlier, only now the allowed k's are quantized. Since synchronism must be achieved between the beam and mode phase velocities, the discrete k's are problematic only at large λ/b or λ/L values.

The propagating wave is more accurately described by a Gaussian mode than by a plane wave [9]. It is realistic to assume Gaussian-type solutions in the y-z plane. These are characterized by a minimum spot size with diameter w_0. The waist at a distance z is defined by

$$w^2(z) = w_0^2\left[1 + \left(\frac{z\lambda}{\pi w_0^2}\right)^2\right]. \tag{20}$$

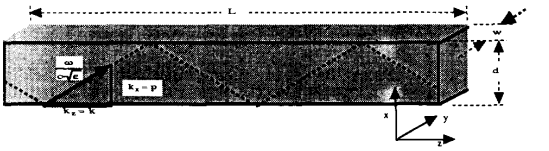

Fig. 6. A schematic of the dielectric film dimensions and coordinate system. The ray optic view of wave propagation is illustrated with the wavenumber decomposed into x and z components.

The minimum w_o is obtained from $\partial w(z)/\partial w_0 = 0$,

$$w_{o}\ \min = \sqrt{\frac{\lambda L}{2\pi}}. \tag{21}$$

This mode waist gives a good estimate of the transverse extent of the optical mode. A well-confined, stable resonator mode should have its waist at resonator center ($z = 0$). To eliminate diffraction effects, the end aperture must physically accommodate the beam divergence. Thus, a minimum resonator width is established:

$$w \gtrsim \sqrt{\frac{L\lambda}{\pi}}. \tag{22}$$

Mode Confinement

The degree of mode confinement in the x-z plane can be obtained by invoking the ray optic picture of guided wave propagation. A guided ray propagates along the resonator via successive reflections at the two interfaces. A schematic of this ray is included in Fig. 6. When the critical angle for total internal reflection (TIR) is satisfied at both interfaces, the mode is well confined. In reality, the wave penetrates into the region above the guide a distance on the order of $1/q$. For TM modes, the effective mode width is

$$d_{\text{eff}} = d + \frac{1}{qr} \text{ where } r = \left(\frac{ck}{\omega n_1}\right)^2 + \left(\frac{ck}{\omega}\right)^2 - 1. \tag{23}$$

A well-confined mode has d_{eff} very close to d; however, the CML relies on the evanescent tail above the guide for electron-mode coupling. A compromise must be reached between low-loss guiding and mode–electron communication.

Mirrors

A high resonator quality factor relaxes the material loss and laser gain requirements of the FEL. One way of improving the Q is to increase the mirror reflectivities. Only integral mirrors are treated. They eliminate the losses associated with coupling out of the guide while offering the advantage of mechanical integrity. Several different mirror designs are shown in Fig. 7 and discussed below. The flexibility of mirror design enables us to choose the reflectivities we require for optimum CML performance.

The simplest Fabry–Perot cavity is formed by cleaving and polishing the ends of the dielectric resonator. The dielectric–air interface can provide sufficient reflectivity r to achieve threshold. Typical r values are about 30–40% for Si, GaAs, and Ge. If an improved r is desired, metal can easily be evaporated onto the end face. The skin depth for radiation penetrating into metal is $\delta = (\lambda/\pi\mu c\sigma)^{1/2}$ in MKS units [10]. For aluminum in the

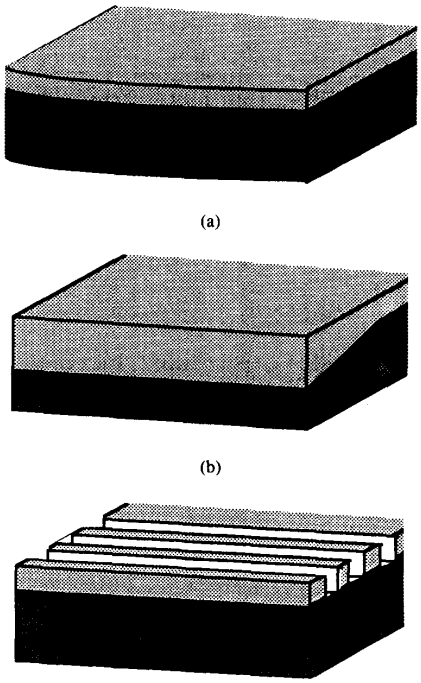

Fig. 7. Three possible mirror designs are shown schematically. (a) Slight curvature is introduced to match the Gaussian-mode wavefront and improve transverse confinement. (b) Adiabatic confinement of the evanescent mode ensures that the end mirrors reflect the entire mode. (c) The square profile distributed Bragg reflector is illustrated. Alternate cross sections and varying index materials exhibit similar pass and stopbands which can be employed as a reflector.

FIR this corresponds to the range 10–160 nm. A 200 nm layer of Al should provide near 100% reflection over the entire range of interest.

Curving the end-mirrors improves mode confinement, eliminating the "walk off" associated with planar mirrors. We assume a Gaussian beam with a minimum waist at resonator-center and match its radius of curvature R. For the most confined mode,

$$R\left(z = \frac{L}{2}\right) = z\left[1 + \frac{\pi w_0^2}{\lambda z^2}\right]_{w_0 = w_{\min}} = L. \tag{24}$$

This is the condition for a confocal cavity.

Since some of the radiation is not confined to the guide, it is naïve to assume that all the guided radiation is reflected by the end face. If the guide is thickened adiabatically, the guided wave is slowed, and the evanescent tail is shortened. The mode is pulled into the dielectric where it is more effectively reflected. Note that the reverse is accomplished if the guiding layer is thinned adiabatically: the wave is accelerated and the evanescent tail grows until the entire wave is launched into the vacuum. We quantify "adiabatic" by assuming that the change occurs over a minimum of 10 wavelengths. This is a practical distance for the entire FIR region.

Another possible reflector is a periodic grating which could be fabricated on the resonator ends. It is known as a distributed Bragg reflector (DBR). Its dispersion relation exhibits pass and stop bands; where there is no solution for a given frequency, the wave cannot propagate and will be reflected.

Materials

In traditional Cerenkov FEL's the guiding medium has been a low-index dielectric. The threshold energy required for lasing, V_T, is determined by the dielectric constant. The gain usually peaks at about twice that voltage. A higher index reduces the voltage required to reach the Cerenkov threshold and also reduces the voltage necessary to operate at a given wavelength. This reduction in energy facilitates the search for an appropriate electron beam source. It also reduces the charging problems associated with high voltage beams. The choice of a semiconductor guiding layer grew from the search for a higher index material, but has become an engineering advantage. Techniques common to integrated circuit [11] and micromechanics structure fabrication [12] provide the basis for constructing the resonators proposed here. Because the dimensions are large relative to integrated circuits, lithography will not be a limiting factor. Rather, control of film deposition and etching will be the principle fabrication issue.

We intend to tailor the material for desired applications. Because semiconductor resonators have not been studied previously in this context, and because some salient points are unearthed, the mechanisms for loss in semiconductors are discussed below.

Losses

In the FIR, radiation and scattering losses are minimal, so we need only consider absorption. Semiconductor absorption is dominated by interband absorption. The threshold wavelength for this is given by

$$\lambda_g[\mu\text{m}] = 1.24/E_g[\text{eV}]. \tag{25}$$

This gap wavelength separates the absorption into two regions. The first corresponds to $\lambda < \lambda_g$ where intrinsic carriers are excited across the bandgap. This is a region of strong absorption which is avoided by a judicious choice of material. The second $\lambda > \lambda_g$ is characterized by free-carrier absorption, lattice absorption, intraband absorption, and defect or dopant absorption. Since FIR radiation satisfies this condition in Si, GaAs, and Ge, we need to address each of these absorption mechanisms.

- *Free-carrier absorption* is a consideration at any temperature in the FIR. Energy is lost as free carriers are first excited, and then transfer energy to the surroundings via scattering [13]. The Classical Drude theory expression for free-carrier absorption is:

$$\alpha_{fc} = \frac{Nq^2\lambda^2}{8\pi^2 m^* nc^3 \tau} \tag{26}$$

where N is the free-carrier concentration, λ is the lasing wavelength, m^* is the free-carrier effective mass in the semiconductor, n is its index of refraction, and τ is the scattering lifetime. This absorption is less significant at low temperatures and short wavelengths.

- *Lattice absorption* must also be considered for infrared wavelengths at most temperatures [14]. It will be increasingly important for very lightly doped semiconductor resonators at wavelengths in the vicinity of 10 μm, where free-carrier absorption has diminished. Excitation of semiconductor resonator

lattice phonon modes via coupling to the beam or the emitted laser radiation is clearly possible in crystalline resonators, and is proportional to a power of the lasing wavelength. The exponent of λ can vary between 1.5 and 2.5, depending upon whether acoustic or optical phonon modes are excited. Polycrystalline or amorphous resonators may be necessary to overcome crystalline lattice absorption limitations [15].

- *Intraband absorption* can be important in p-type semiconductors [16]. As with free-carrier absorption, the absorption coefficient is proportional to the free hole concentration. However, this mechanism relies upon penetration of the hole quasi-Fermi level into one or more of the valence bands. Such penetration indicates degenerate doping, which high-resistivity materials avoid. In n-type semiconductors [17], absorption is usually below the limit of free-carrier absorption, except at wavelengths a few microns longer than the direct band-gap absorption edge.
- *Impurity absorption* [18] will be unimportant at temperatures near 300 K. However, near 77 K, freeze-out of free carriers onto dopant impurity sites will allow the reverse process to occur via absorption of photons with energy near the impurity ionization energy. Thus, if temperature lowering is used as a means to control dielectric constant, this mechanism will need consideration.

An ideal resonator would have low losses in the FIR and a tunable dielectric constant ϵ. Clearly both are attainable with a semiconductor resonator. To reduce losses we should choose a high resistivity material since the resistivity is a good indication of the number of free carriers available for absorption. It is also possible to freeze out the carriers to reduce absorption. The index (or equivalently ϵ), depends on temperature, carrier concentration, and wavelength. Clearly there is potential for control of the desirable properties given careful consideration of the material preparation.

IV. Design Characteristics of the CML

The general theory of the Cerenkov laser and the further design constraints imposed by resonator optics fix the characteristics of the CML. First, since the relative dielectric constants of Si, GaAs, and Ge are 11.8, 12.9, and 16.0, the Cerenkov threshold energies

$$V_T = (\gamma_T - 1)mc^2 \tag{27}$$

are 23.1, 21.0, and 16.8 kV, respectively. The relative gain g_o peaks at about $2V_T$ and the coupling factor f_c will tend to further shift the maximum point toward higher energies. Thus, overall, operation with V_b = 50–100 kV is anticipated. Electrons in this energy range can be produced either with conventional cathode materials such as LaB_6, or a high-brightness field-emitting cathode structure. In the first case, achieving suitable current densities would require approximately 10:1 compression of the beam thickness. If a high-brightness cathode is employed, very little beam compression would be needed. Both options lie within the range of parameters that typify modern low-total-current high-current-density high-brightness (low-energy-spread) electron gun design.

In order to further constrain the design, it is useful to estimate the parameter values needed to fix g, the gain per pass, at g = 1. Assuming that a round beam is employed and matched to the resonator waist:

$$\sigma_{by} = \sigma_{bx} \tag{28a}$$

$$w \sim \sqrt{\frac{\lambda L}{2\pi}} \tag{28b}$$

When the energy and coupling parameter are fixed, the overall gain scaling is given by

$$g \sim \frac{J_{bo} L^{5/2}}{\lambda^{1/2}}. \tag{29}$$

If we fix L/λ at, say, 10^2, then at V_b = 100 kV the current density required to achieve g = 1 is

$$J_b(g = 1) = \frac{463}{L^2}\ \mathrm{A/cm^2}. \tag{30}$$

Values for J_b are tablulated in Table I. The current density at 100 μm is high, but within attainable limits for well-focused short-path beams. Furthermore, if the $L/\lambda = 10^2$ limit is increased, the required current density drops quickly. When the constraint μ_c = 4 is also enforced, the total beam cross-section scales with λ and the total current is I_b = 360 μA. It will be the same for all cases listed in Table I.

The maximum allowable energy spread is also the same for all cases. When $\lambda/L = 10^{-2}$, the electron voltage spread is $(\delta V_{beam}/V_{beam}) = 2.6\%$. Energy spreads which are a factor of 5 to 10 lower than this are possible in practice, and thus this constraint is modest.

It is also interesting to consider the potential operating efficiency. A single-particle calculation indicates that a typical electron will lose between 1 and 10% of its energy. This elementary one-dimensional estimate does not predict where in the beam profile the saturation profile will be located. Experience with similar devices, however, indicates that the single-particle estimate is typical. It is also possible in principle to operate the CML with a collector which is biased near the cathode potential. In this case, the overall efficiency can be considerably above the electronic efficiency $[\delta\gamma/(\gamma - 1)]$.

V. Conclusion

The theory and calculations presented indicate the feasibility of the CML. The criteria for achieving unity gain per pass are modest, and certainly substantially above the threshold limit established by material losses and output coupling. Gain well-above unity is obtainable at the shorter wavelengths, suggesting the possibility of a CML amplifier. In fact, there are a number of implications for device modifications beyond the simple planar resonator treated.

Alternate macroscopic configurations would enhance the gain and efficiency. One possibility is the klystron. It consists of two short film sections, one to initiate velocity modulation and a second to extract energy from the bunched beam. The drift section separating the films can take a number of forms including a cut-off guide, lossy guide, or the introduction of dispersive magnetic fields. A wedged film can be used in any configuration to slow the phase velocity of the wave to match the electron loss and thus enhance the electronic efficiency.

The use of a semiconducting film lends itself to even more innovative designs. The advantage of wavelength tunability has been one of the motivating forces behind FEL development. The coefficient for ϵ-tuning in the range of interest is approximately $\Delta\lambda/\Delta\epsilon \approx 0.2$. The dielectric constant for semiconductors can be tuned via a number of mechanisms including applying a voltage or changing the temperature. Photolithography

allows for essentially limitless (on the CML scale) implementation of resonator designs which we plan to develop in the future.

REFERENCES

[1] J. Walsh, K. Felch, K. Busby, R. Layman, and D. Kapilow, "Cerenkov radiation in dielectric-lined waveguides," *Appl. Phys. Lett.*, vol. 38, pp. 601–603, 1981.

[2] S. Von Laven, J. Walsh, J. Branscum, J. Golub, and R. Layman, "High-power Cerenkov maser oscillator," *Appl. Phys. Lett.*, vol. 41, pp. 408–410, 1982.

[3] E. Garate, J. Walsh, S. Moustaizis, J.-M. Buzzi, C. Rouille, H. Lamain, and B. Johnson, "Cerenkov maser operation at 1–2 mm wavelengths," *Appl. Phys. Lett.*, vol. 48, pp. 1326–1328, 1986.

[4] E. Garate, C. Shaughnessy, and J. Walsh, "High-gain Cerenkov free-electron laser at far-infrared wavelengths," *IEEE J. Quantum. Electron.*, vol. QE-23, pp. 1627–1632, 1987.

[5] J. Walsh, K. Felch, K. Busby, and R. Layman, "Cerenkov and Cerenkov-Raman masers: Experiments," in *Proceedings of the Summer School on the Physics of Quantum Electronics*, vol. 7, S. Jacobs and M. Scully, Eds. Reading, MA: Addison Wesley, 1980, pp. 301–322.

[6] J. Walsh, "Stimulated Cerenkov radiation," in *Advances in Electronics and Electron Physics*, C. Marton, Ed. New York: Academic, 1982, vol. 58, pp. 271–310.

[7] J. C. Slater, *Microwave Electronics*. New York: Dover, 1969, p. 48.

[8] B. Johnson, "An infrared Cerenkov laser," Dartmouth College, Ph.D. dissertation, 1985.

[9] D. Marcuse, *Theory of Dielectric Optical Waveguides*. New York: Academic, 1974.

[10] J. D. Jackson, *Classical Electrodynamics, 2nd Ed.* New York: Wiley, 1975, p. 225.

[11] S. Sze, *VLSI Technology*, 2nd ed. New York: McGraw-Hill, 1988.

[12] K. Gabriel, J. Jarvis, and W. Trimmer, "Small machines, large opportunities: A report on the emerging field of microdynamics," presented at Rep. NSF Workshop Microelectromechan. Syst. Res., Salt Lake City, UT, July 27, 1987.

[13] J. I. Pankove, *Optical Processes in Semiconductors*. New York: Dover, 1971, p. 75.

[14] W. G. Spitzer, "Multiphonon lattice absorption," in *Semiconductors and Semimetals*, vol. 3 (Optical Properties of III–V Compounds), R. K. Willardson and A. C. Beer, Eds. New York: Academic, 1967, p. 17ff.

[15] P. C. Taylor, "Optical properties of noncrystalline semiconductors," in *Noncrystalline Semiconductors*, vol. 1, M. Pollak, Ed. Boca Raton, FL: CRC, 1987, p. 19.

[16] J. I. Pankove, *Optical Processes in Semiconductors*. New York: Dover, 1971, p. 67.

[17] ——, *Optical Processes in Semiconductors*. New York: Dover, 1971, p. 71.

[18] ——, *Optical Processes in Semiconductors*. New York: Dover, 1971, p. 62.

E. Fisch, photograph and biography not available at the time of publication.

Albert K. Henning (M'79), photograph and biography not available at the time of publication.

J. Walsh, photograph and biography not available at the time of publication.